Activation of methane by gold cations: Guided ion beam and theoretical studies

Feng-Xia Li and P. B. Armentrout[a)]
Chemistry Department, University of Utah, 315 South 1400 East, Room 2020, Salt Lake City, Utah 84112

(Received 21 April 2006; accepted 12 June 2006; published online 4 October 2006)

The potential energy surface for activation of methane by the third-row transition metal cation, Au^+, is studied experimentally by examining the kinetic energy dependence of this reaction using guided ion beam tandem mass spectrometry. A flow tube ion source produces Au^+ primarily in its $^1S_0$ ($5d^{10}$) electronic ground state level but with some ^3D (and perhaps higher lying) excited states that can be completely removed by a suitable quenching gas (N_2O). Au^+ ($^1S_0$) reacts with methane by endothermic dehydrogenation to form $AuCH_2^+$ as well as C–H bond cleavage to yield AuH^+ and $AuCH_3^+$. The kinetic energy dependences of the cross sections for these endothermic reactions are analyzed to give 0 K bond dissociation energies (in eV) of $D_0(Au^+–CH_2)=3.70\pm0.07$ and $D_0(Au^+–CH_3)=2.17\pm0.24$. *Ab initio* calculations at the B3LYP/HW+/6-311++G(3*df*,3*p*) level performed here show good agreement with the experimental bond energies and previous theoretical values available. Theory also provides the electronic structures of the product species as well as intermediates and transition states along the reactive potential energy surface. Surprisingly, the dehydrogenation reaction does not appear to involve an oxidative addition mechanism. We also compare this third-row transition metal system with the first-row and second-row congeners, Cu^+ and Ag^+. Differences in thermochemistry can be explained by the lanthanide contraction and relativistic effects that alter the relative size of the valence *s* and *d* orbitals. © *2006 American Institute of Physics*. [DOI: 10.1063/1.2220038]

I. INTRODUCTION

Since Haruta *et al.* discovered that nanoscale gold deposited on a transition metal oxide substrate such as TiO_2 is very active for room temperature oxidation of carbon monoxide, special attention has been given to the use of these clusters in catalysis.[1] Chen and Goodman recently identified a two atomic layer thick gold structure as the form responsible for the catalysis observed.[2] This interesting chemistry finds parallels in the gas phase where Chowdhury and Wilkins found that gold cations reacted at thermal energies with a number of aliphatic and aromatic hydrocarbons using Fourier-transform ion cyclotron resonance (FTICR) spectrometry.[3] Indeed, it has been found that third-row transition metal elements are much more reactive with alkanes than first- and second-row metals,[4–10] observations similar to those in solution-phase C–H bond activation chemistry.[11] Covalent metal–CH_x bond energies are much stronger to the third-row metals than those to metals of the first and second rows because of the lanthanide contraction that alters the relative sizes of the valence *s* and *d* orbitals.[12] The lanthanide contraction is a consequence of 4*f* shielding and relativistic effects.

As part of an ongoing project to more fully understand the activation of H–H, H–C, and C–C bonds, we have extended our studies of the reactions of atomic transition metal ions with small hydrocarbons to third-row metals.[13–17] Numerous studies of the reactions of atomic transition metal ions (M^+) with hydrogen and small hydrocarbons have been conducted in the gas phase, where they are free from effects of solvent, stabilizing ligands, and metal support.[18,19] These studies provide insight into the electronic requirements for the activation of C–C, C–H, and H–H bonds by transition metal ions in addition to establishing periodic trends for transition metals involved in these reactions. Among the methods used for such studies, guided ion beam mass spectrometry (GIBMS) has the ability to determine accurate bond dissociation energies (BDEs) for $M^+–C_xH_y$ ($x=0–3$, $y=0–2x+2$). This thermochemistry is of obvious interest and is relevant to the study of catalytic reactions involving transition-row elements.[20,21] Such gas-phase experiments are most complete for first-and second-row elements, although studies of third-row transition elements now include a number of experimental[3–5,9,10,13–17,22–29] and theoretical[4,12,23–26,30–37] studies.

In this study, we report results for the reactions of Au^+ with CH_4 and CD_4 over a wide range of kinetic energies. Using FTICR spectrometry, Irikura and Beauchamp[4,5] found that several of the third-row transition metal ions (Ta^+, W^+, Os^+, Ir^+, and Pt^+) react exothermically to dehydrogenate methane, $M^+ + CH_4 \rightarrow MCH_2^+ + H_2$. The exceptions are the early metals, La^+ and Hf^+, along with Re^+ and Au^+, although Au^+ was found to slowly dehydrogenate ethane.[5] The relative inactivity of Au^+ can be attributed largely to the stable, filled 5*d* shell electron configuration, $5d^{10}$.[10] Thermochemistry relevant to the present work comes from Chowdhury and Wilkins, whose bracketing studies suggested lower limits of $D(Au^+–CH_2)>4.12$ eV and $D(Au^+–CH_3)>2.43$ eV.[3]

a)Electronic mail: armentrout@chem.utah.edu

Irikura and Goddard later reinterpreted Chowdhury and Wilkins's experiments to suggest that a lower limit of $D(Au^+-CH_2)>4.01$ eV is more likely,[23] and recently Aguirre *et al.* established an *upper* limit of $D(Au^+-CH_2)\leq 3.86\pm0.03$ eV in a photodissociation experiment.[29]

These disparate values can be checked in the present work as the GIBMS technique allows us to examine endothermic processes, probe the potential energy surface, and provide mechanistic information complementary to previous experimental and theoretical work. Theoretical calculations are also performed to assign electronic structures and explore potential energy surfaces and possible mechanisms. Two points are of particular interest. Despite having a closed shell configuration, Au^+ ($^1S_0, 5d^{10}$) does react with methane. Because of the closed shell, the mechanism for the reaction differs from the other third-row transition metal cations.

II. EXPERIMENT AND THEORY

A. Instrumentation

The guided ion beam tandem mass spectrometer on which these experiments were performed has been described in detail previously.[38,39] Briefly, reactant ions are generated in a direct current discharge flow tube source described below. The ions are extracted from the source, accelerated, and focused into a magnetic sector momentum analyzer for mass selection of the primary reactant ions. Mass-selected ions are decelerated to a desired kinetic energy and focused into an octopole ion beam guide, which uses radio-frequency electric field to trap the ions in the radial direction and ensure complete collection of reactant and product ions.[40,41] The octopole passes through a static gas cell that contains the reaction partner (here CH_4 and CD_4) at a low pressure (usually $\leq$0.3 mTorr) so that multiple ion-molecule collisions are improbable. All products reported here result from single bimolecular encounters, as verified by pressure dependence studies. Product and unreacted primary ions drift to the end of the octopole where they are extracted, focused, passed through a quadrupole mass filter for mass analysis, and subsequently detected with a secondary electron scintillation ion detector using standard pulse counting techniques. Ion intensities are converted to absolute cross sections after correcting for background signals.[42] Absolute uncertainties in cross section magnitudes are estimated to be ±20%.

The kinetic energy dependence of the ions is varied in the laboratory frame by scanning the dc bias on the octopole with respect to the potential of the ion source region. Ion kinetic energies in the laboratory frame, E_{lab}, are converted to energies in the center-of-mass frame, $E_{c.m.}$, using the formula $E_{c.m.}=E_{lab}m/(m+M)$, where m and M are the neutral and ionic reactant masses, respectively. All energies reported below are in the c.m. frame unless otherwise noted. Two effects broaden the cross section data: the thermal motion of the neutral reactant gas (Doppler broadening)[43] and the kinetic energy distribution of the reactant ion. The absolute zero and distribution of the ion kinetic energies are determined using the octopole guide as a retarding potential analyzer as described previously.[42] The distribution of ion kinetic energies is nearly Gaussian and has a typical full width at half maximum (FWHM) between 0.5 and 0.8 eV (laboratory) in these studies. The uncertainties in the absolute energy scale are ±0.05 eV (laboratory).

B. Ion source

Atomic gold metal cations are formed in a direct current discharge flow tube (dc/FT) source.[39] This source consists of a cathode held at high negative voltage (0.7–1.5 kV) over which a flow of approximately 90% He and 10% Ar passes at a total pressure of 0.3–0.5 Torr and ambient temperature. The cathode in this work is gold-plated aluminum. Ar^+ ions created in the discharge are accelerated toward the metal cathode, thereby sputtering Au^+ ions. These ions are then swept down a 1 m long flow tube. The flow conditions used in this ion source provide about 10^5 thermalizing collisions between an ion and He ($\sim10^4$ collisions with Ar) before the ions enter the guided ion beam apparatus. Excited states of Au^+ are observed to survive these flow conditions, although the populations of these states vary appreciably, suggesting that small amounts of contaminant gases can effectively quench them. Excited species that react exothermically with methane are easily removed by introducing CH_4 into the flow tube about 15 cm downstream of the discharge zone at a pressure of ~100 mTorr, but this leaves at least one excited species, as will be seen below. Complete quenching of all excited states can be achieved by the addition of N_2O as a cooling gas, as demonstrated below. Details of this reaction are provided elsewhere[44] but rely on the fact that all states of Au^+ except the $^1S_0$ ground state react exothermically with N_2O to form $AuO^+ + N_2$.

C. Data analysis

The kinetic energy dependence of product cross sections is analyzed to determine E_0, the energy threshold for product formation at 0 K. The apparent threshold observed under laboratory conditions can lie below E_0 because of the kinetic and internal energy distributions of the reactants. To determine E_0, endothermic reaction cross sections are modeled using Eq. (1),[45–47]

$$\sigma(E)=\sigma_0\sum g_i(E+E_i+E_{el}-E_0)^n/E, \quad (1)$$

where σ_0 is an energy-independent scaling factor, E is the relative kinetic energy of the reactants, E_{el} is the electronic energy of the Au^+ reactant, and n is an adjustable parameter. There is an explicit sum of contributions from rovibrational states of reactants at 300 K, denoted by i, having energies E_i and populations g_i, where $\Sigma g_i=1$. The various sets of vibrational frequencies and rotational constants used to determine E_i in this work are taken from the literature for CH_4 and CD_4.[48] Before comparison with the experimental data, Eq. (1) is convoluted with the kinetic energy distributions of the ions and neutral reactants at 300 K. The σ_0, n, and E_0 parameters are then optimized using a nonlinear least-squares analysis to give the best reproduction of the data.[46,47] Error limits for E_0 are calculated from the range of threshold values for different data sets over a range of acceptable n values combined with the absolute uncertainty in the kinetic energy scale.

D. Theoretical calculations

In general, quantum chemistry calculations reported here are computed using the B3LYP hybrid density-functional method[49,50] and performed with the GAUSSIAN 98 and GAUSSIAN 03 suites of programs.[51,52] The B3LYP functional was used for all the calculations done here because it provides reasonable results for the analogous W^+, Hf^+, Re^+, Ir^+, and Pt^+ with CH_4 systems.[13–17] In all cases, the thermochemistry reported here is corrected for zero-point energy effects using unscaled frequencies. Because several of the transition states of interest here involve bridging hydrogens, the rather large 6-311++G($3df$,$3p$) basis set is used for carbon and hydrogen. This basis set gives good results for the thermochemistry of methane and dihydrogen, with deviations from experiment of less than 0.08 eV for the bond energies of $H–CH_3$ (4.406 versus 4.480 eV), $H_2–CH_2$ (4.666 versus 4.713 eV), H–CH (4.332 versus 4.360 eV), C–H (3.532 versus 3.465 eV), and H–H (4.505 versus 4.478 eV). (See Table 1 of Ref. 17 for experimental thermochemistry used for all H, D, CH_x, and CD_x species.) The 60 core electrons of gold are described by the relativistic effective core potential (ECP) of Hay-Wadt (HW),[53] with the valence electrons described by the Los Alamos double-zeta (LANL2DZ) basis set. This basis set is optimized for neutral atoms, whereas the positive charge differentially contracts the *s* orbitals compared to the *d* orbitals. Hence, calculations were performed with an altered HW-ECP basis set for Au^+ as described by Ohanessian *et al.* (HW+).[12]

The most appropriate choice for a level of theory has been thoroughly investigated for the first- and third-row transition metal methyl cations by Holthausen *et al.*[32] and for first-row transition metal methylene cations by Holthausen *et al.*[54] In the first study, these authors used B3LYP, Becke-half-and-half-LYP (BHLYP), and QCISD(T) methods with a basis set consisting of a polarized double-zeta basis on C and H and the Hay-Wadt relativistic ECP with valence electrons added. The symmetries of the metal methyl species were constrained to C_{3v}. For the first-row MCH_3^+ species (M=Sc–Cu), where experimental results are available for all metals,[19] these authors conclude that the B3LYP functional overbinds, with a mean absolute deviation (MAD) from experiment of 0.41 eV. The BHLYP functional and the QCISD(T) methods perform more accurately, with MADs of 0.18 and 0.20 eV, respectively. For the third-row elements, the bond energies calculated using B3LYP were again higher than those for BHLYP and QCISD(T). In contrast, for the metal methylene complexes,[54] the BHLYP functional predicts bond energies consistently below experimental values, whereas the performance of the B3LYP functional is quite good. In addition, these authors found that the results depended on the basis set used for the metal ion with an all electron basis providing better results than ECP methods. On the basis of these results, the present study includes calculations for the various product ions using the B3LYP and BHLYP functionals with both the HW+ and Stuttgart/Dresden (SD) ECP (Ref. 55) for Au^+, along with QCISD(T)/HW+ calculations. Such calculations will be explicitly noted, but unless otherwise designated, our results will refer to a B3LYP/HW+/6-311++G($3df$,$3p$) level of theory.

Using the HW+ basis set and the B3LYP level of theory, we calculate a $^1S_0$ ground state for Au^+, with a ^3D state at 2.36 eV. The excitations to the lowest lying triplet state were found to be 2.81, 2.44, 2.87, and 2.48 eV for the B3LYP/SD, BHLYP/HW+, BHLYP/SD, and QCISD(T)/HW+ combinations of theoretical method/basis set, showing that the atomic excitations are not strongly dependent on the choices made. These calculated triplet excitation energies can be favorably compared to the experimental value of 2.29 eV (statistically weighted mean of all spin-orbit levels).[56] Note that the results obtained using the HW+ basis set agree somewhat better with experiment than the SD results.

III. EXPERIMENTAL RESULTS

Figure 1 shows cross sections for the reaction of Au^+ with CD_4, which yields product ions as shown in reactions (2)–(4).

$$Au^+ + CD_4 \rightarrow AuD^+ + CD_3 \quad (2)$$

$$\rightarrow AuCD_3^+ + D \quad (3)$$

$$\rightarrow AuCD_2^+ + D_2. \quad (4)$$

Studies of the reaction of Au^+ with CH_4 were also performed and yielded results consistent with those shown in Fig. 1. Only results from the perdeuterated species are presented here because the use of CD_4 reduces mass overlap and allows intensities of the various product ions to be measured more accurately over a great energy range. $AuCD^+$ and AuC^+ are not observed in this system, despite a careful search for these two products. The cross sections for these products are unlikely to exceed 10^{-18} cm^2 over the range of energies examined.

Results for the reaction of Au^+ with CD_4 obtained when the ions are quenched with N_2O in the flow tube are shown in Fig. 1(a). As confirmed by related studies of the reaction of Au^+ with O_2,[44] N_2O efficiently quenches the excited states of Au^+, leaving only the $^1S_0$ ($5d^{10}$) ground state. Thus, the three product channels of reactions (2)–(4) all exhibit single featured cross sections with no reactivity observed at the lowest energies, consistent with the previous ICR studies by Chowdhury and Wilkins[3] and by Irikura and Beauchamp[4,5] in which no thermal reactions were observed. $AuCD_2^+$ formed in reaction (4) has the lowest threshold observed, beginning at about 0.7 eV. Formations of AuD^+ and $AuCD_3^+$ arise from similar apparent thresholds near 2.0 eV, which indicates that the $Au^+–D$ and $Au^+–CD_3$ single bonds have similar bond energies. However, formation of AuD^+ dominates the product spectrum at high energies because of angular momentum effects,[22,57–59] as discussed below. At energies greater than ~2.5 eV, the $AuCD_2^+$ cross section begins to decline. This decline corresponds well with the apparent thresholds of the other two products observed; however, only the cross section of AuD^+ is large enough to account for the initial drop in intensity of $AuCD_2^+$. From this, we infer that

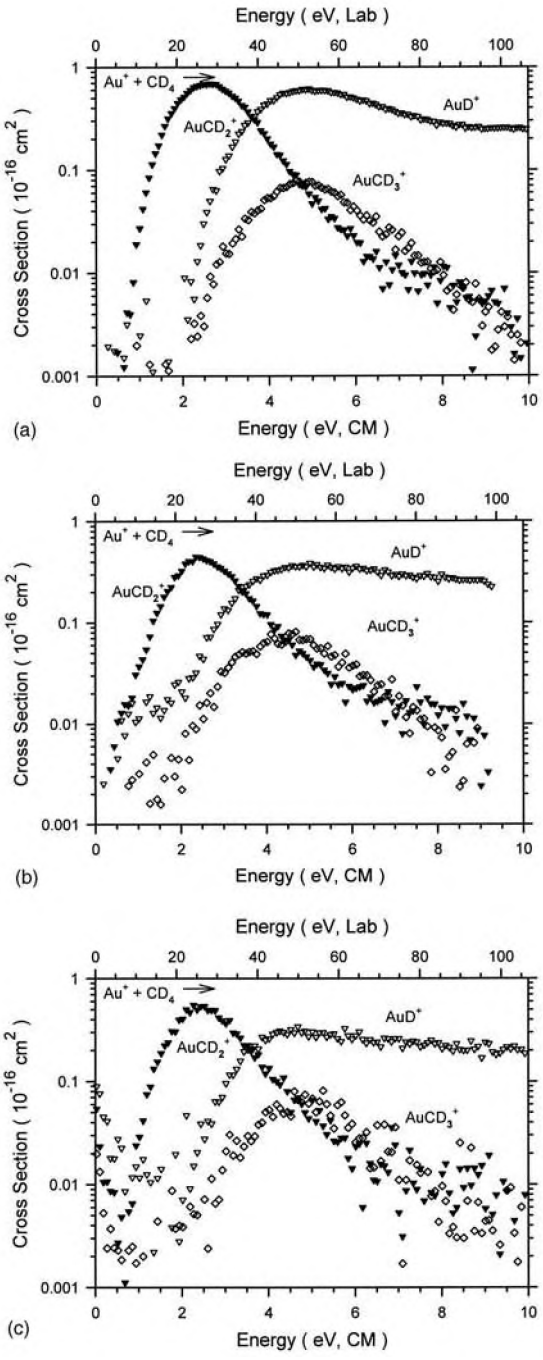

FIG. 1. Cross sections for reaction of Au^+ with CD_4 as a function of kinetic energy in the center-of-mass frame (lower axis) and laboratory frame (upper axis). Results are shown for Au^+ produced with N_2O (a), CH_4 (b), and no quenching gases (c) added to the flow tube source.

either there is a decomposition reaction of $AuCD_2^+ \rightarrow AuD^+ + CD$ or that the formation of $AuD^+ + CD_3$ is competitive with the formation of $AuCD_2^+ + D_2$. Because decomposition of $AuCD_2^+$ to AuD^+ cannot occur until much higher energies, reactions (2) and (4) must be competitive with each other. Such competition is most easily explained if these two products share a common intermediate, as discussed below. The kinetic energy dependences of all three product cross sections are analyzed using Eq. (1) and the results are compiled in Table I.

Figure 1(b) shows results for the same reactions but with Au^+ formed with CH_4 as a quenching gas in the flow tube. The qualitative character of the three cross sections remains the same, but all three exhibit a low energy feature starting at about 0.2 eV. This suggests that an excited electronic state of Au^+ is now present. If we compare the magnitudes of the $AuCD_2^+$ cross sections at elevated energies, we find that the Au^+ (CH_4 quench) data average $70\% \pm 20\%$ that of the Au^+ (N_2O quench) data. Thus, the amount of excited state present in the Au^+ (CH_4 quench) beam is estimated as $30\% \pm 20\%$. Interestingly, whereas the relative magnitudes of the AuD^+ cross sections follow a similar trend, the $AuCD_3^+$ cross section magnitudes are essentially the same, indicating that the branching ratio between reactions (2) and (3) is different for the different states involved. Note that the absolute magnitudes of the low energy features in all three product ion cross sections are about 10–20 times smaller than those of the analogous ground state cross sections. This comparison implies that the excited states are less reactive than the Au^+ ($^1S_0$) ground state by a factor of 1–10. Furthermore, it can be seen that the magnitudes of the $AuCD_2^+$ and AuD^+ cross sections in the threshold region are similar, suggesting that the relative efficiency of dehydrogenation for the excited states is drastically reduced compared to the ground state reactivity.

Identification of the excited state may be achieved by comparing the thresholds for the reactions of Au^+ ($^1S_0$) with those for Au^+ (CH_4 quench). For the AuD^+ and $AuCD_3^+$ reactions, we note that the only states of Au^+ that do not have excitation energies that exceed the thresholds for Au^+ ($^1S_0$) reactivity, 2.65 eV (Table I), are the $^3D_3$ ($6s^15d^9$) and $^3D_2$ ($6s^15d^9$) states at 1.865 and 2.187 eV.[56] The $^3D_1$ ($6s^15d^9$) and $^1D_2$ ($6s^15d^9$) excited states lie 3.442 and 3.673 eV, respectively, above the ground state.[56] Indeed, analysis of the AuD^+ and $AuCD_3^+$ cross sections in the threshold regions of the Au^+ (CH_4 quench) data finds thresholds of 0.48 ± 0.12 and 0.44 ± 0.20 eV, respectively (Table I). These thresholds lie an average of 2.18 ± 0.20 eV lower in energy than those for reaction of Au^+ ($^1S_0$), a value that agrees nicely with the excitation energy of the $^3D_2$ state. We surmise that the $^3D_3$ state is probably present as well but masked by the lower threshold of the $^3D_2$ state.

In contrast to the threshold shifts observed for AuD^+ and $AuCD_3^+$, the threshold for $AuCD_2^+$ shifts by only 0.73 ± 0.11 eV, a value that does not correspond to any electronically excited state of Au^+. On the basis of the threshold for $AuCD_2^+$ determined for reaction of Au^+ ($^1S_0$), formation of this product by the ^3D excited states present is exothermic. Thus, the threshold observed here must correspond to a barrier along the potential energy surface for the $^3D_2$ excited state, a hypothesis that is investigated theoretically below. It should also be noted that reactions (2) and (3) also exhibit essentially identical thresholds to reaction (4) for the Au^+ (CH_4 quench) data (Table I), indicating that they may be limited by the same rate-limiting step.

Without any quenching gas, Fig. 1(c), Au^+ reacts to yield the same three reaction products having cross sections with the main features remaining similar to those of Figs. 1(a) and 1(b). Comparison of the magnitudes at elevated energies of these main features suggests that the Au^+ beam formed with

TABLE I. Parameters of Eq. (1) used in modeling the reaction cross sections.

Reactants	Products	σ_0	n	E_0 (eV)	$D_0(Au^+-L)$ (eV)
$Au^+ + CH_4$[a]	$AuH^+ + CH_3$	0.3±0.1	1.1±0.1	2.54±0.08	1.94±0.08
	$AuCH_2^+ + H_2$	1.1±0.1	1.7±0.2	0.96±0.05	3.75±0.05
	$AuCH_3^+ + H$	0.04±0.01	1.2±0.3	2.57±0.13	1.91±0.13
$Au^+ + CD_4$[a]	$AuD^+ + CD_3$	1.0±0.3	1.3±0.2	2.65±0.08	1.93±0.08
	$AuCD_2^+ + D_2$	1.0±0.2	1.5±0.1	1.15±0.05	3.67±0.05
	$AuCD_3^+ + D$	0.12±0.02	1.4±0.2	2.64±0.12	1.94±0.12
$Au^+ + CD_4$[b]	$AuD^+ + CD_3$	0.03±0.01	1.3[c]	0.48±0.12	
	$AuCD_2^+ + D_2$	0.05±0.01	1.5[c]	0.42±0.10	
	$AuCD_3^+ + D$	0.003±0.001	1.4[c]	0.44±0.20	

[a]Au^+ ($^1S_0$) data as quenched with N_2O.
[b]Data for Au^+ quenched with CH_4.
[c]Held to the value used to analyze the Au^+ ($^1S_0$) data.

no quenching gas contains about 30%–40% excited states. At low energies, all three cross sections exhibit features that decline with increasing kinetic energy, corresponding to exothermic reactivity. These exothermic features must correspond to the $^3D_1$, $^1D_2$, or higher lying states as all of these have sufficient energy to render reactions (2)–(4) exothermic. Compared to the Langevin-Gioumousis-Stevenson (LGS) collision cross section,[60] the exothermic reactivity ranges from 1000 to 14 000 times smaller, such that species comprising only 0.10%–0.007% of the beam could account for the observed low energy reactivity. Note that the exothermic feature is now dominated by AuD^+ formation, with $AuCD_2^+$ smaller by a factor of 3±1 and $AuCD_3^+$ smaller by a factor of 8±5.

IV. THERMOCHEMICAL AND THEORETICAL RESULTS

The endothermic cross sections for each product ion are analyzed using Eq. (1), as described above, and the optimum values of the parameters are listed in Table I. Because this model explicitly includes rotational, translational, and vibrational energy distributions, all E_0 thresholds determined by Eq. (1) correspond to 0 K values. From the measured thresholds, the BDEs of the gold-ligand cations can be calculated using Eq. (5),

$$D_0(Au^+ - L) = D_0(R - L) - E_0, \tag{5}$$

where the $D_0(R-L)$ values can be calculated using the heats of formation summarized previously.[17] This equation assumes that there are no activation barriers in excess of the endothermicity of a given reaction, an assumption that is often true for ion-molecule reactions because of the long-range attractive forces.[42,47] Table II provides a summary of the BDEs derived and a comparison with literature values, as discussed below. Tables S1 and S2 provide summaries of the B3LYP theoretical results (energies and structures) for each of the product ions and their excited states.[61] These results are discussed in detail in the following sections for each species.

A. Au^+-H

We have recently measured the AuH^+ bond energy as 2.17±0.08 eV from the reactions of Au^+ with H_2 and D_2.[62] From Eq. (5), $D_0(D-CD_3)=4.58$ eV, and a calculated zero-point energy difference between AuD^+ and AuH^+ of 0.039±0.004 eV, this predicts a threshold of 2.37±0.08 eV for formation of AuD^+ in reaction (2). Our analysis of this cross section (Table I) measures a somewhat higher threshold of 2.65±0.08 eV. Similarly, the predicted E_0 value for the AuH^+ product ion obtained in the CH_4 system is 2.31±0.08 eV, whereas the measured threshold is 2.54±0.08 eV. Thus, the CH_4 and CD_4 systems behave similarly but do not agree with the thermodynamic results obtained from the H_2 and D_2 systems. On average, the thresholds in the methane systems are higher in energy by 0.26±0.16 eV, a discrepancy that can be attributed to a competitive shift. Reaction (4) strongly competes with reaction (2) at its threshold, whereas there are no competing channels in the reactions of Au^+ with H_2 and D_2. This competition can delay the apparent onset for formation of AuD^+ (AuH^+) in the methane systems.

As shown in Table II and discussed elsewhere,[62] previous theoretical results give bond energies lower than our experimental value of 2.17±0.08 eV. Our calculations find BDEs of 2.07 (1.80) eV when using the B3LYP functional, 1.66 (1.43) eV for BHLYP, and 1.66 eV for QCISD(T) using the HW+(SD) basis sets on Au. As found by Holthausen *et al.* for the third-row transition metal ion methyl cations,[32] the B3LYP functional overbinds compared to the BHLYP and QCISD(T) methods. In this system, the B3LYP calculation is in good agreement with our experimental result.

The $^2\Sigma^+$ ground state has a valence electronic configuration of $1\sigma_b^2 1\pi^4 1\delta^4 2\sigma^1$, where σ_b represents the bonding orbital and the remaining are nonbonding orbitals on the metal with the 2σ being largely 6*s*. The bond length determined here at the B3LYP/HW+ level (Table S2), 1.553 Å, is in good agreement with values from Ohanessian *et al.*, 1.539 Å,[12] and Ishikawa *et al.*, 1.56 Å.[36] We also determined excitation energies and geometries for $^2\Delta$ and $^2\Pi$ excited states, as described in detail elsewhere.[62]

TABLE II. Comparison of experimental and theoretical thermochemistry for AuH^- and $AuCH_x^-$ (x=0–3) species.

	This work						Previous work	
		Theory[a]						
		B3LYP		BHLYP		QCISD(T)		
Species	Expt.	HW+	SD	HW+	SD	HW+	Expt.	Theory
Au^-–H ($^2\Sigma^-$)	2.17±0.08[b]	2.07	1.80	1.66	1.43	1.66		0.59,[c] 1.45[d] 1.83,[e] 1.96[f]
Au^-–CH_3 ($^2A_1$)	2.17±0.24	2.22	2.04	1.73	1.60	1.93	>2.43[g]	1.91,[h] 2.22,[i] 1.97±0.22[i,j] 1.68±0.22[i,j]
Au^-–CH_2 ($^1A_1$)	3.70±0.07	3.69	3.50	3.00	2.86	3.29	≥4.12[g] >4.01[l] ≤3.86±0.03[m]	3.86±0.30[i,k] 3.92[h] 3.76[n]
Au^-–CH ($^2A'$)		3.43	3.24	2.79	2.67	3.04		4.08[k]
Au^-–C ($^1\Sigma^-$)	≥3.19±0.08[o]	3.03	2.75	1.89	1.68	2.77	3.36±0.04[m]	3.47[p]

[a]Calculations using the indicated level of theory with the 6-311++G(3df,3p) basis set on C and H and the indicated ECP and basis set on Au^- (see text).
[b]Reference 62.
[c]Reference 36.
[d]Reference 12.
[e]Reference 71.
[f]Kaldor and Hess, as reported in Ref. 72.
[g]Reference 3.
[h]Reference 37.
[i]Reference 32 [B3LYP, BHLYP, and QCISD(T), respectively].
[j]Empirically corrected value.
[k]Reference 23.
[l]Reinterpreted in Ref. 23 from results in Ref. 3.
[m]Reference 29.
[n]Reference 31.
[o]Reinterpreted in the present study from results in Ref. 29 (see text).
[p]Reference 63.

B. Au^+–CH_3

The BDE of Au^+–CD_3 determined from the CD_4 system is 1.94±0.12 eV and the BDE of Au^+–CH_3 from the CH_4 system is 1.91±0.13 eV. After correcting for the zero-point energy differences in these two values (0.032 eV), we obtain a weighted average of 1.91±0.18 eV for the BDE of Au^+–CH_3. Because this value is similar to the BDE of Au^+–H obtained from a routine analysis of the AuH^+ and AuD^+ channels (1.92±0.11 eV), this confirms that a single bond to Au^+ is formed in each molecule. As noted above, because there is competition with the dehydrogenation reaction, the BDE of AuH^+ determined from methane systems is somewhat low and a similar result seems likely for $AuCH_3^+$. However, we can use the competitive shift determined for AuH^+ (0.26±0.16 eV) to give our best estimate of the $AuCH_3^+$ bond energy as 2.17±0.24 eV. This is equivalent to measuring that the thresholds for $AuCH_3^+$ ($AuCD_3^+$) are the same as those for AuH^+ (AuD^+). Previously, Chowdhury and Wilkins determined a lower limit for $D_0(Au^+–CH_3)$ of 2.43 eV on the basis of observing a minor reaction (21%) of laser-ablated Au^+ with CH_3I in their FTICR spectrometer.[3] The disagreement with the thermochemistry measured here indicates that their observations of exothermic reactivity are associated with the reactions of electronically or translationally excited gold ions.

As mentioned above, Holthausen *et al.* carefully considered the most appropriate choice for a level of theory for the first- and third-row transition metal methyl cations.[32] B3LYP, BHLYP, and QCISD(T) levels of theory gave predicted Au^+–CH_3 bond energies (D_e) of 2.22, 1.76, and 1.53 eV, respectively. On the basis of results for the first-row metal methyl cations compared with experimental values, empirical corrections of +0.22 and +0.16 eV were applied to the BHLYP and QCISD(T) results, leading to final estimated bond energies (D_e) of 1.97 and 1.68 eV with estimated errors of ±0.22 eV. Another theoretical value of 1.91 eV was determined by Hrušák at the CCSD(T)-QR level.[37] These previous theoretical values are somewhat below our adjusted experimental value of 2.17±0.24 eV and close to the uncorrected value (1.91±0.18 eV), but nearly within the uncertainties of both.

Our B3LYP/HW+ and BHLYP/HW+ calculations reproduce the results of Holthausen *et al.*,[32] whereas our QCISD(T)/HW+ value is considerably higher, 1.93 versus 1.53 eV. If the empirical corrections suggested by Holthausen *et al.* are applied to our values, we obtain 2.22 (B3LYP/HW+), 1.95 (BHLYP/HW+), and 2.09 (QCISD(T)/HW+) eV for Au^+–CH_3, in good agreement with our adjusted experimental value. The use of the SD ECP decreases our predicted BDEs to 2.04 (B3LYP) and 1.60 (BHLYP) eV. Note that the bond energies for AuH^+ and $AuCH_3^+$ in both the experimental and theoretical results are similar (depending on the level of theory, differences of 0.07–0.27 eV), consistent with both having comparable

single covalent metal-ligand bonds. Thus, whatever the origin of any discrepancy between experiment and any particular level of theory, the same discrepancy is occurring for both AuH^+ and $AuCH_3^+$.

We find the ground state of $AuCH_3^+$ to be $^2A_1$ with C_{3v} symmetry, consistent with previous work.[32] The Au–C and C–H bond lengths (2.113 and 1.086 Å) and AuCH bond angles (102.3°) calculated here (B3LYP/HW+, Table S2) are comparable to those from Holthausen *et al.* [2.114 and 1.092 Å and 102.1° B3LYP; 2.125 and 1.083 Å and 101.7°, BHLYP; 2.105 and 1.091 Å and 103.0°, QCISD(T)].

C. $Au^+–CH_2$

The BDE of $Au^+–CD_2$ determined from the CD_4 system is 3.67±0.05 eV and the BDE of $Au^+–CH_2$ from the CH_4 system is 3.75±0.05 eV (Table I). After correcting for the zero-point energy differences in these two values (0.030 eV), we obtain a weighted average of 3.70±0.07 eV for the BDE of $Au^+–CH_2$. Chowdhury and Wilkins studied the reactions of Au^+ with several organic molecules in a FTICR spectrometer.[3] They determined a lower limit for D_0 of 4.12 eV on the basis of a minor reaction (6%) of laser-ablated Au^+ with CH_3I. However, this assignment has been questioned by Irikura and Goddard[23] because even a small amount of electronically or translationally hot ions could form the product $AuCH_2^+$.[23] Irikura and Goddard suggest that a more conservative lower limit is 4.01 eV, on the basis of the analogous major reaction (70%) between Au^+ and CH_3Br, but again this result could be influenced by the presence of excited ions. In contrast to these lower limits, Aguirre *et al.* determined an upper limit of 3.86±0.03 eV by studying the gas-phase photodissociation of $AuCH_2^+$.[29] This value is nicely consistent with our experimental value.

Irikura and Goddard previously calculated that $AuCH_2^+$ has a $^1A_1$ ground state.[23] Their calculation characterizes the metal-carbon bond as nearly a pure dative bond in which the $^1A_1$ state of CH_2 donates its lone pair of electrons into the empty 6*s* orbital on Au^+, and there is a π backbonding contribution that is 80% $5d\pi$ in character. They calculate D_e=3.35 eV and include an empirical correction of 0.52±0.30 eV, leading to a corrected D_0 of 3.86±0.30 eV, in good agreement with our experimental result. However, their final recommended 0 K bond energy of 4.08±0.09 eV comes from the limits of 4.01 and 4.12 eV from Chowdhury and Wilkins's experiment, as discussed above. Irikura and Goddard also located a $^3A_1$ excited state that lies 3.02 eV above the $^1A_1$ ground state. Heinemann *et al.* calculated a $^1A_1$ ground state with a BDE of 3.76 eV using a quasirelativistic LDA+B density-functional calculation.[31] Their calculation found that the relativistic contribution accounts for more than 70% of the total bond energy in $AuCH_2^+$. A BDE of 3.92 eV was determined by Hrušák at the CCSD(T)-QR level.[37] These latter BDEs are also in reasonable agreement with our experimental result.

The present calculations, B3LYP/HW+ (SD), also find a $^1A_1$ ground state with a bond energy of 3.69 (3.50) eV, in good agreement with our experimental value. The BHLYP and QCISD(T) values, 3.00 (2.86) and 3.29 eV, are much too low. Our ground state geometry of r(Au–C)=1.903 Å, r(C–H)=1.090 Å, and ∠AuCH=121.9° (Table S2) differs somewhat from those calculated by Irikura and Goddard using GVB 2/4 (MR-CISD) levels, r(Au–C) =2.034(1.889) Å, r(C–H)=1.082(1.099) Å, and ∠AuCH =123.3°(122.3°),[23] and by Heinemann *et al.*, r(Au–C) =2.153 Å, r(C–H)=1.104 Å, and ∠AuCH=123.7°.[31]

The $^1A_1$ ground state of $AuCH_2^+$ has a valence electronic configuration of $(1a_{1b})^2(1b_{1b})^2(1b_2)^2(2a_1)^2(1a_2)^2(3a_1)^2$, where the $1a_{1b}$ and $1b_{1b}$ orbitals are bonding, the $1b_2$, $2a_1$, and $1a_2$ orbitals are 5*d* nonbonding orbitals on Au, and the $3a_1$ orbital is a nonbonding 6*s*-5*d*σ hybrid orbital on Au. Our calculations also located $^3B_1$ ($^3A'$) and $^3A_1$ excited states lying 1.31 and 3.42 eV higher in energy than the ground state (Table S1). The $^3B_1$ ($^3A'$) and $^3A_1$ excited states have valence electronic configurations of $(1a_{1b})^2(1b_{1b})^2(1b_2)^2(2a_1)^2(1a_2)^2(3a_1)^1(2b_1^*)^1$ and $(1a_{1b})^2(1b_{1b})^2(1b_2)^2(2a_1)^2(1a_2)^2(3a_1)^1(4a_1^*)^1$, respectively, where $4a_1^*$ is an antibonding σ orbital and $2b_1^*$ is an antibonding π orbital. The $^3B_1$ state is found to have an imaginary frequency (an umbrella motion) that distorts the molecule to form the $^3A'$ state. Thus, before any zero-point energy corrections, the $^3A'$ is more stable than $^3B_1$ by 0.005 eV; however, the zero-point energy exceeds the height of the barrier such that this state dynamically has C_{2v} symmetry. We also find two singlet excited states, $^1B_1$ and $^1A_2$, lying 1.44 and 4.63 eV higher in energy, respectively, although both are heavily spin contaminated. These excited states have valence electronic configurations of $(1a_{1b})^2(1b_{1b})^2(1b_2)^2(2a_1)^2(1a_2)^2(3a_1)^1(2b_1)^1$ and $(1a_{1b})^2(1b_{1b})^2(1b_2)^2(2a_1)^2(1a_2)^1(3a_1)^2(4a_1^*)^1$, respectively.

D. $Au^+–CH$

Irikura and Goddard estimate a value of 4.08 eV for the $Au^+–CH$ bond energy after estimating an intrinsic bond strength and correcting for promotion and exchange energies.[23] The present calculations, B3LYP/HW+ (SD) and QCISD(T), find a $^2A'$ ground state with bond energies of 3.43 (3.24) and 3.04 eV, much lower than the estimated value. The BHLYP values, 2.79 (2.67) eV, are even lower.

Our calculations find that the $^2A'$ state has a bent geometry (Table S2). The valence orbital occupation is $1\sigma_b^2 1\pi_b^4 1\delta^4 2\sigma^2 2\pi^{*1}$ given in terms of the equivalent $C_{\infty v}$ symmetry designations, where the C(2*s*) orbital is excluded for simplicity, the $1\sigma_b$ orbital is a bonding combination of the $2p_z$(C) and $5d_{z2}$(Au) orbitals, the $1\pi_b$ orbitals are the expected $2p_{x,y}$(C)-$5d_{xz,yz}$(Au) bonding molecular orbitals, the 1δ are pure metal $5d_{xy,x2-y2}$(Au) orbitals, the 2σ orbital is a nonbonding 6*s*-$5d_{z2}$ hybrid (largely a torus surrounding the bonding axis), and the $2\pi^*$ is a $2p_{x,y}$(C)-$5d_{xz,yz}$(Au) antibonding molecular orbital. When the occupied $2\pi^*$ is in the plane of the molecule (a' symmetry), the molecule bends, ∠AuCH=141°. When the $2\pi^*$ (a'') orbital is occupied, a $^2\Pi(A'')$ state lying only 0.11 eV higher in energy is formed and has ∠AuCH=180° (Table S2).

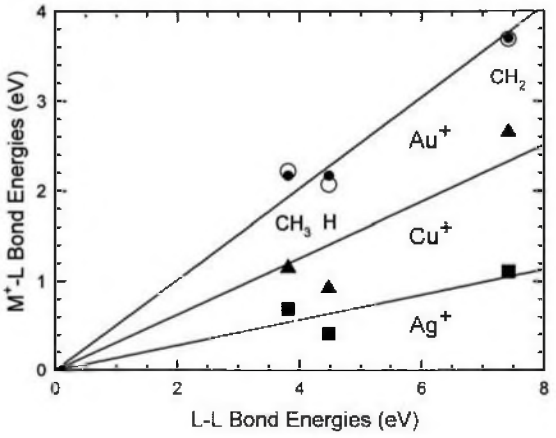

FIG. 2. Correlation of Au^+-L bond energies with those for the organic analogs. $L-L$. Au^+-L values are from Table II and include both experiment (closed circles) and theory (open circles). Data for Cu^+ and Ag^+ (taken from Refs. 19 and 64–68) are shown by the triangles and squares. The lines are linear regression fits to the experiment data constrained to pass through the origin to emphasize the bond-order correlations.

E. Au^+-C

In their gas-phase photodissociation study of $AuCH_2^+$, Aguirre *et al.* observed that Au^+ and AuC^+ were both formed with identical thresholds of 3.86±0.03 eV.[29] Assuming that photodissociation of $AuCH_2^+$ occurs at the thermodynamic thresholds, these onsets imply that $D_0(Au^+-C)$ =3.36±0.04 eV. However, if we combine $D_0(AuC^+-H_2)$ ≤3.86±0.03 eV with $D_0(Au^+-CH_2)$=3.70±0.07 eV from our experiment, this gives a lower limit of $D_0(Au^+-C)$ ≥3.19±0.08 eV.

The present calculations, B3LYP/HW+ (SD) and QCISD(T), find a $^1\Sigma^+$ ground state for AuC^+ with bond energies of 3.03 (2.75) and 2.77 eV, with BHLYP values, 1.89 (1.68) eV, being even lower. These values are somewhat below that calculated by Barysz and Pyykkö at the CCSD(T) level (3.47 eV).[63]

Our theoretical calculations find the ground state of AuC^+ to be $^1\Sigma^+$ with a Au–C bond length of 1.809 Å (Table S2). The $^1\Sigma^+$ ground state of AuC^+ has a valence electronic configuration of $1\sigma_b^2 1\pi_b^4 1\delta^4 2\sigma^2$, where the orbitals are comparable to those described above for $AuCH^+$. The lowest lying excited state is $^3\Pi$ lying 0.63 eV higher in energy and has a $1\sigma^2 1\pi^4 1\delta^4 2\sigma^1 2\pi^{*1}$ configuration. Another excited state is $^3\Phi$ ($1\sigma^2 1\pi^4 1\delta^3 2\sigma^2 2\pi^{*1}$) lying 3.26 eV above the ground state. In both excited states, the AuC bond length increases, consistent with occupation of the antibonding $2\pi^*$ orbital.

On the basis of the experimental values of AuH^+, $AuCH_2^+$, and $AuCH_3^+$, the BHLYP functional with MADs of 0.55 (HW+) and 0.72 (SD) eV provides less accurate predictions compared to the B3LYP functional with MADs of 0.05 (HW+) and 0.23 (SD) eV, whereas the QCISD(T) values are in between the other two methods with a MAD of 0.39 eV using the HW+ ECP for Au. Clearly, the B3LYP values are in good general agreement with experiment for this metal ion.

F. Bond-energy bond-order correlation for Au^+-CH_x bonds

One interesting way of investigating the bond order of simple metal-ligand species is to compare with organic analogs, i.e., $D_0(Au^+-L)$ vs $D_0(L-L)$. Such a plot is shown in Fig. 2. It can be seen that the correlation indicates that Au^+-H and Au^+-CH_3 are single bonds, and $Au^+=CH_2$ is a double bond, as confirmed by theory. (The linear regression line in Fig. 2 is constrained to include the origin to emphasize the bond-order correlation of AuL^+ versus L_2 species.) Also illustrated in Fig. 2 is the relatively reasonable agreement between experiment and theory: B3LYP for all species.

It is also interesting to compare these results to those for the first- and second-row congeners, Cu^+ and Ag^+. Bond energies for CuH^+, $CuCH_2^+$, and $CuCH_3^+$ are 0.92±0.13, 2.65±0.05, and 1.15±0.07 eV, respectively.[19,64–66] The analogous species for Ag^+ have bond energies of 0.41±0.06, ≥1.11±0.04, and 0.69±0.05 eV, respectively.[67,68] From this comparison, we find that the first- and second-row transition metal bonded species of Cu^+ and Ag^+ are much weaker than the corresponding third-row congeners. On average, the linear regression lines indicate that the bonds to Au^+ are 62% greater than those to Cu^+ and 258% greater than those to Ag^+, a consequence of the relativistic effect and lanthanide contraction.

V. POTENTIAL ENERGY SURFACES OF [Au,C,4H]$^+$

We construct the potential energy surfaces (Figs. 3 and 4) for interaction of Au^+ with methane at the B3LYP/HW+/6-311++G(3*df*,3*p*)level of theory and include zero-point energy corrections (unscaled). In most cases, we located transition states using relaxed potential energy surface scans along reasonable reaction pathways, followed by geometry optimization and frequency calculations to confirm the transition states. In some cases, we also used the synchronous transit-guided quasi-Newton method (QST3).[69,70] As discussed above, the B3LYP level of theory reproduces the bond energies of Au^+-CH_x species adequately. Thus the relative characteristics of these surfaces are likely to be qualitatively correct and are of the most interest here. Tables S3 and S4 provide summaries of the theoretical results (energies and structures) for each of the intermediates and transition states.[61] Figures 5 and 6 illustrate the structures of these intermediates and transition states on the singlet and triplet spin surfaces, respectively.

A. Singlet surface

The interaction of methane with the singlet ground state of Au^+ ($^1S_0$,$5d^{10}$) leads initially to the formation of a $Au^+(CH_4)$ adduct (^1A) in which the methane molecule distorts by extending one of the C–H bonds as the C–H bond begins to break (Fig. 5). This intermediate is calculated to lie 1.04 eV below the Au^+ ($^1S_0$)+CH_4 ground state reactants and is the global minimum. We also located a symmetric $^1A_1$ excited state, which is found to have an imaginary frequency that distorts the molecule to form the ^1A state. Thus, before any zero-point energy corrections, the $^1A_1$ is more stable than

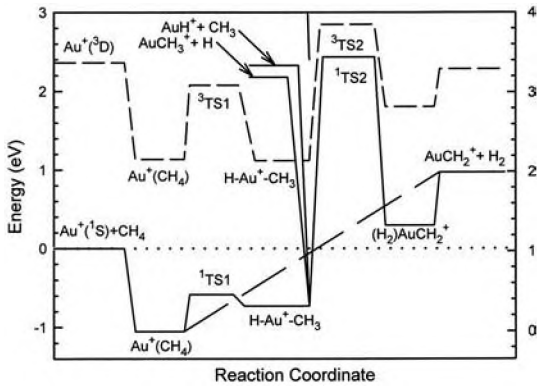

FIG. 3. $[Au,C,4H]^-$ potential energy surfaces derived from theoretical results at the B3LYP/HW/6-311++G($3df,3p$) level (see Table S3). Singlet and triplet surfaces are indicated by the full and dashed lines, respectively. Energies on the left are relative to the Au^- ($^1S_0$)+CH_4 ground state asymptote, whereas those on the right are referenced to the $Au^-(CH_4)$(^1A) intermediate. The long dashed line schematically shows the results of the relaxed potential energy surface scan given in Fig. 4 more quantitatively.

^1A by 0.002 eV; however, the zero-point energy exceeds the height of the barrier such that this state dynamically has C_{2v} symmetry.

Upon further reduction of the Au–H bond distance, the system passes over a transition state, ^{1}TS1 (^1A) with a HAuC bond angle of 54°, and leads to the insertion intermediate H–Au^+–CH_3. The singlet $HAuCH_3^+$ ($^1A'$) intermediate has C_s symmetry, a HAuC bond angle of 85°, and a HAuCH dihedral angle of 180°. The Au–H and Au–C bond distances, 1.540 and 2.095 Å, respectively, are comparable to those of AuH^+($^2\Sigma^+$), 1.553 Å, and $AuCH_3^+$($^2A_1$), 2.113 Å. This observation along with the Au–C–H bond angles of ~100° indicate that the methyl group is covalently bound to Au in this state. Upon rotation of 60° to a HAuCH dihedral angle of 0°, there is a $^1A'$ transition state lying 0.008 eV higher in energy, where the imaginary frequency of 120 cm^{-1} corresponds to the rotation back to the $^1A'$ ground state.

Continuing along the singlet surface, the $(H_2)AuCH_2^+$($^1A_1$) intermediate is reached via ^{1}TS2, a transition state (Fig. 5) lying 2.43 eV above ground state reactants

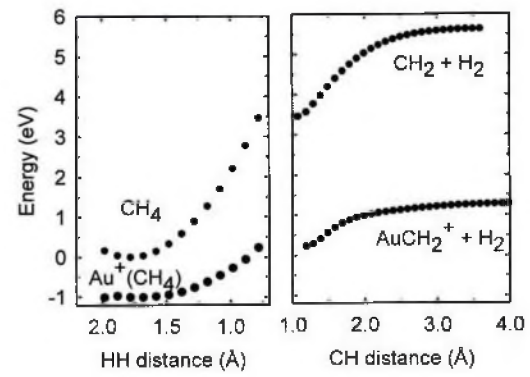

FIG. 4. Relaxed potential energy surface scan along the singlet surface for dehydrogenation of $Au^-(CH_4)$ and CH_4 derived from theoretical results at the B3LYP/HW+/6-311++G($3df,3p$) level. The energies are relative to the Au^-($^1S_0$)+CH_4 ground state asymptote. On the left, the surface for bringing two hydrogen atoms to within 0.8 Å are shown, whereas the right panel shows removal of H_2 from this distorted methane.

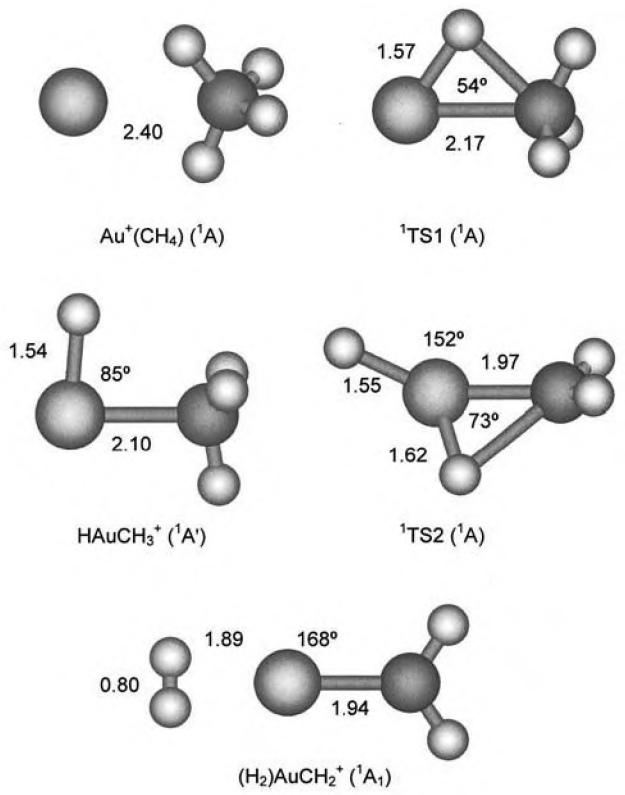

FIG. 5. Structures of several intermediates and transition states along the singlet surface of the $[Au,C,4H]^-$ system calculated at the B3LYP/HW+/6-311++G($3df,3p$) level of theory. Bond lengths shown are in angstroms and HAuC bond angles are in degrees.

and 3.16 eV above the $HAuCH_3^+$ intermediate. Intrinsic reaction coordinate (IRC) calculations verify that this transition state connects the $HAuCH_3^+$($^1A'$) and $(H_2)AuCH_2^+$($^1A_1$) intermediates. The $(H_2)AuCH_2^+$($^1A_1$) intermediate is planar and has a H_2 bond distance of 0.795 Å compared to free H_2 at 0.742 Å. The Au–C bond distance, 1.940 Å, is close to that of $AuCH_2^+$($^1A_1$), 1.903 Å. It lies 0.30 eV above the ground state reactants. The $(H_2)AuCH_2^+$($^1A_1$) intermediate can easily dissociate by losing H_2, a dissociation that costs 0.68 eV. Overall, the $AuCH_2^+$($^1A_1$)+H_2 product asymptote lies 0.97 eV above the ground state reactants, which can be favorably compared with the experimental threshold of 0.96±0.05 eV.

The singlet potential energy surface characterized thus far is limited by ^{1}TS2 at 2.43 eV (Table S3), well above our experimental threshold of only 0.96±0.05 eV for $AuCH_2^+$ +H_2 products, but only slightly below our experimental thresholds of 2.54±0.08 and 2.57±0.13 eV for AuH^++CH_3 and $AuCH_3^+$+H products, respectively. Thus ^{1}TS2 cannot be the limiting transition state in the observed dehydrogenation reaction (4). Several attempts to locate a lower energy ^{1}TS2 state did not succeed nor could a pathway involving a $(H)_2AuCH_2^+$ intermediate be found. Because the ground state Au^+ ion has a $5d^{10}$ electron configuration, it is not surprising that this ^{1}TS2 has such a high energy because this transition state involves multiple bond formation (Fig. 5). Likewise this explains why a $(H)_2AuCH_2^+$ intermediate could not be located.

In searching for a low energy path for dehydrogenation,

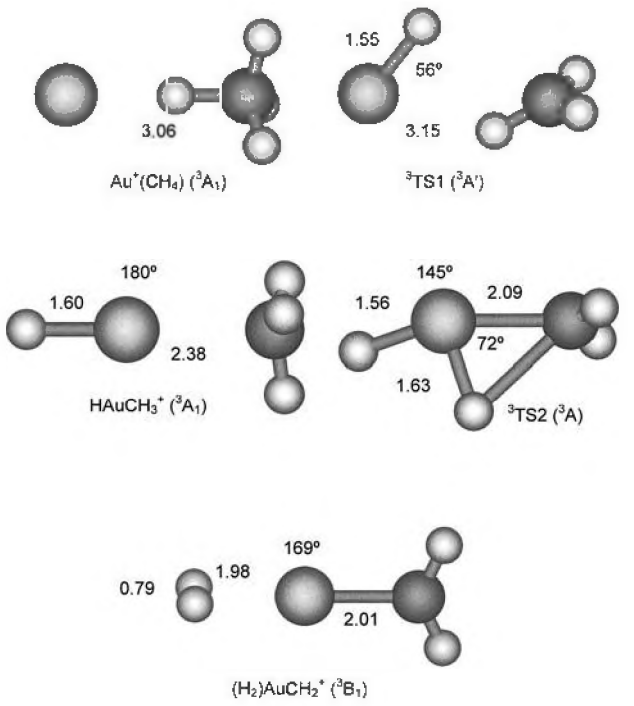

FIG. 6. Structures of several intermediates and transition states along the triplet surface of the $[Au,C,4H]^+$ system calculated at the B3LYP/HW+/6-311++G(3*df*,3*p*) level of theory. Bond lengths shown are in angstroms and HAuC bond angles are in degrees.

we also considered whether the reaction can proceed from the $Au^+(CH_4)(^1A)$ adduct directly to H_2 and $AuCH_2^+(^1A_1)$ products without any transition states involved. Thus, we performed a relaxed potential energy surface scan starting with the $Au^+(CH_4)(^1A)$ adduct in which the H–H distance between the two hydrogens closest to Au^+ is decreased. Results of this calculation are shown in Fig. 4 and end once the H–H distance decreases to about 0.78 Å, close to the bond distance of free H_2. At this point, another relaxed potential energy surface scan increases the C–H distance, leading to $AuCH_2^+ + H_2$ (Fig. 4). It can be seen that this pathway allows for dehydrogenation of methane without any barrier in excess of the overall endothermicity. For comparison, we also performed a similar set of relaxed potential energy surface scans for CH_4 in the absence of Au^+ (Fig. 4), where the product asymptote is $CH_2(^1A_1)+H_2(^1\Sigma_g^+)$ in order to conserve spin. The comparison of the surfaces with and without Au^+ shows that the metal ion lowers the energy of the entire surface, in particular, by stabilizing the CH_2 product.

B. Triplet surface

Interaction of Au^+ ($^3D,6s^15d^9$) with methane leads initially to the formation of a $Au^+(CH_4)$ adduct in which the metal lies along one of the C–H bonds (Fig. 6). This adduct is in a $^3A_1$ state (C_{3v} symmetry) lying 1.14 eV above the ground state reactant asymptote. Note that the $Au^+–CH_4$ bond energies are comparable, 1.22 and 1.04 eV for the $^3A_1$ and ^1A states, respectively. Upon activation of the C–H bond, the system passes over a transition state, ^{3}TS1, leading to the insertion intermediate $H–Au^+–CH_3$. This transition state has C_s symmetry ($^3A'$ state) and a HAuC bond angle of 56.0° (Fig. 6). On the triplet surface, the $HAuCH_3^+$ intermediate is a $^3A_1$ state (C_{3v} symmetry) and has a HAuC bond angle of 180° (Fig. 6). In this molecule, the Au–H bond distance, 1.602 Å, is slightly longer than that of $AuH^+(^2\Sigma^+)$, 1.553 Å, whereas the Au–C bond distance of 2.381 Å is much longer than that of $AuCH_3^+(^2A_1)$, 2.113 Å. Thus, this intermediate is essentially a AuH^+ molecule with a loosely bound CH_3 group because the triplet spin means that there is no covalent coupling between the unpaired electrons on each group. A $^3A'$ excited state of this intermediate was also located having C_s symmetry, a HAuC bond angle of 141°, and a HAuCH dihedral angle of 0°. Upon rotation to a HAuCH dihedral angle of 180°, there is a $^3A'$ transition state lying 0.01 eV higher in energy, having a rotational motion with an imaginary frequency of 208 cm^{-1}.

Continuing along the triplet surface, the $(H_2)AuCH_2^+(^3B_1)$ intermediate is reached via ^{3}TS2 (Fig. 6), lying 2.85 eV above ground state reactants and 1.73 eV above the $HAuCH_3^+$ intermediate. The ^{3}TS2 lies only 0.42 eV above the ^{1}TS2 state and has a similar geometry (Figs. 5 and 6). The $(H_2)AuCH_2^+$ intermediate lies 0.56 eV below the triplet reactants and has C_{2v} symmetry with a H_2 bond distance of 0.786 Å, comparable to that of H_2, 0.742 Å. The geometry of the $AuCH_2^+$ part of the molecule is similar to that for $AuCH_2^+(^3B_1)$ (Fig. 6). Overall, this is consistent with the weak $H_2–AuCH_2^+$ bond energy, calculated to be only 0.48 eV relative to the $AuCH_2^+(^3B_1)+H_2$ asymptote. A $^3A_1$ excited state of the $(H_2)AuCH_2^+$ intermediate also having C_{2v} symmetry was located but is very high in energy, 2.57 eV higher than the $^3B_1$ state. This excited state has a very long $Au–H_2$ bond length, 3.53 Å, and a very short H_2 bond length, 0.744 Å, consistent with a very weak interaction. Indeed, this state has an imaginary frequency (21 cm^{-1}) corresponding to a CAuH bend, which breaks the symmetry and allows this state to collapse to the $^3B_1$ state.

VI. DISCUSSION

σ-bond activation by atomic metal ions can usually be explained using a simple donor-acceptor model. Such reactions require electronic configurations in which there is an empty acceptor orbital on the metal ion into which the electrons of a bond to be broken are donated. Concomitantly, metal electrons in orbitals having π symmetry backdonate into the antibonding orbital of the bond to be broken. If the acceptor orbital is occupied, a repulsive interaction can result, leading to inefficient reaction either by more direct abstraction pathways or by introduction of a barrier to the reaction. In our previous studies, the activation of methane by atomic metal ions was explained by this simple donor-acceptor model, which leads to an oxidative addition mechanism. In such a mechanism, oxidative addition of a C–H bond to M^+ forms a $H–M^+–CH_3$ intermediate. Products can be formed by the reductive elimination of H_2 at low energies and by further dehydrogenation of primary products at still higher energies. For first-row transition metal ions,[19] the reductive elimination process proceeds through a four-centered transition state from the $H–M^+–CH_3$ intermediate to a $(H_2)MCH_2^+$ intermediate in which a hydrogen molecule is

electrostatically bound to the MCH_2^+ species. This latter intermediate then decomposes by expulsion of H_2. For the third-row transition metal ions of Ir^+ and Pt^+,[16,17] a $(H)_2MCH_2^+$ intermediate was involved. However, for the reaction of Au^+ with methane, the calculated potential energy surfaces performed here (Figs. 3 and 4) illustrate a different reaction mechanism that does not involve any transition state.

A. Mechanism for dehydrogenation of Au^+ with methane

On the singlet surface, the empty s orbital of Au^+ ($^1S_0$,$5d^{10}$) acts as an efficient acceptor orbital, and a doubly occupied $5d\pi$ orbital can provide an efficient donor orbital. This leads naturally to an intermediate in which Au^+ forms two covalent bonds using $6s5d$ hybrids. Thus, ^{1}TS1 is relatively low in energy and formation of $H-Au^+-CH_3(^1A')$ is exothermic. However, $Au^+(CH_4)(^1A')$ is the global minimum on the potential energy surface because the stable closed shell configuration of Au^+ ($^1S_0$) makes the oxidative addition less favorable than open shell metals.

From $H-Au^+-CH_3(^1A')$, the $(H_2)AuCH_2^+(^1A_1)$ intermediate can be formed which easily loses dihydrogen to form the ground state $AuCH_2^+(^1A_1)+H_2$ products. This process involves the ^{1}TS2 transition state, with an energy of 2.43 eV, which is bigger than our experimental threshold of 0.96 ± 0.05 eV. Because the ground state Au^+ ion has a $5d^{10}$ electron configuration, it is not surprising that this ^{1}TS2 has such a high energy because this transition state involves multiple bond formation (Fig. 5). As shown in Fig. 4, the relaxed potential energy surface scans starting from ground state $Au^+(CH_4)$ adduct (^1A) show that dehydrogenation of methane by $Au^+(^1S_0)$ can occur directly from the $Au^+(CH_4)$ adduct (^1A). Formation of $AuCH_2^+(^1A_1)+H_2$ products occurs directly without any transition states involved. This reaction mechanism is unique among the third-row transition metal systems, which generally have low energy pathways involving $H-M^+-CH_3$ and sometimes $(H)_2MCH_2^+$ intermediates. Even though Au^+ does not undergo oxidative addition and reductive elimination in this process, Fig. 4 demonstrates that Au^+ does lower the energy for the dehydrogenation reaction, making it much more efficient than in the absence of the ion.

B. Mechanism for higher energy products

As the energy available increases above about 2.0 eV, AuH^+ and $AuCH_3^+$ products are formed (Fig. 1). There are two possible pathways for these two product channels. One pathway is bond cleavage from the $Au^+(CH_4)$ adduct or more likely by simple bond cleavages of the $H-Au^+-CH_3$ intermediate. These processes, in particular, formation of $AuH^+ + CH_3$, deplete the population of the $Au^+(CH_4)$ adduct or $HAuCH_3^+$ intermediate such that the cross section for the dehydrogenation process declines commensurately. Because formation of $AuCH_2^+ + H_2$ is thermodynamically preferred by about 1.5 eV (Table II), this indicates that formation of $AuH^+ + CH_3$ must be preferred kinetically. This is consistent with a simple bond cleavage of HAu^+-CH_3 at elevated kinetic energies.

In the reaction of Au^+ with CH_4 (CD_4), the AuH^+ (AuD^+) cross section is dominant at energies above 5 eV (Fig. 1). This is typical behavior for the reaction of bare metal ions with hydrogen-containing polyatomic molecules. The observation that the $AuH^+ + CH_3$ ($AuD^+ + CD_3$) channel dominates the nearly isoenergetic $AuCH_3^+ + H$ ($AuCD_3^+ + D$) channel (Table I) is largely a result of angular momentum constraints.[22,57–59] Briefly, because the $AuCH_3^+ + H$ ($AuCD_3^+ + D$) channel has a reduced mass of 1.0 (2.0) amu, much smaller than that of the reactants, 14.8 (18.2) amu, it can only be formed by reactants that come together with smaller orbital angular momenta, i.e., at small impact parameters. In contrast, the $AuH^+ + CH_3$ ($AuD^+ + CD_3$) channel has a reduced mass of 13.9 (16.5) amu, close to that of the reactants, such that most impact parameters leading to strong interactions between the Au^+ and methane can form these products and still conserve angular momentum. The branching ratio of $\sigma(AuD^+)/\sigma(AuCD_3^+)$ is different when different quenching gases are introduced. The ratio changes from 9 (N_2O quench) to 5 (CH_4 quench) and 6 (no quenching) from threshold to about 5 eV. These ratios are all consistent with the range of 4–20 suggested as appropriate for a statistical mechanism associated with a long-lived intermediate; however, the differing ratios for the different source conditions indicate that different electronic states behave differently for reactions (2) and (3). The lower ratio associated with the excited state reactivity suggests a longer-lived intermediate, which is probably consistent with the deeper well for the $^3A_1$ state of $HAuCH_3^+$ compared with the shallow well for the $^1A'$ state of this intermediate (Fig. 3).

C. Reaction of $Au^+(^3D)$

Experimentally, as seen in Fig. 1(b), reactions of the triplet states of Au^+ have similar thresholds for all three product ions. The thresholds for AuD^+ and $AuCD_3^+$ (0.48 ± 0.12 and 0.44 ± 0.20 eV, respectively, Table I) are consistent with the thermodynamic thresholds expected for reaction of the $^3D_2$ state (0.46 ± 0.08 and 0.45 ± 0.12 eV, respectively), whereas formation of ground state $AuCD_2^+(^1A_1)$ is exothermic from this state. This suggests that the triplet reactants do not couple to the singlet potential energy surface but remain on the excited triplet surface throughout. This still permits formation of ground state $AuH^+(^2\Sigma^+)+CH_3(^2A'')$ and $AuCH_3^+(^2A_1)+H(^2S)$ and their deuterated analogs at their thermodynamic limits, but the dehydrogenation reaction is now endothermic by 0.14 ± 0.07 eV given the experimental $AuCH_2^+(^1A_1)$ bond energy (Table II) and excitation energies of $AuCH_2^+(^3B_1)$ (1.31 eV, Table S1) and $Au^+(^3D_2)$ (2.187 eV). This translates to an endothermicity of 0.22 ± 0.07 eV in the CD_4 system, but this still lies below the experimental threshold of 0.42 ± 0.10 eV (Table I). However, the calculated potential energy suggests that the dehydrogenation reaction on the triplet surface is limited by ^{3}TS2, calculated to lie 0.49 eV above the triplet reactants, which agrees nicely with the observed threshold. Thus, reaction on

the triplet surface appears to occur by formation of a $H-Au^+-CH_3(^3A_1)$ intermediate, which can cleave either the AuH or AuC bonds to yield reactions (2) and (3). Alternatively, the system can dehydrogenate by passing over ^{3}TS2, which lies above the asymptotic energy of the triplet products (Fig. 3). Because this reaction is kinetically limited by this tight transition state having an energy comparable to that of the reaction (2) and (3) asymptotes, this explains why formation of $AuCH_2^+$ on the triplet surface is so much less efficient than on the singlet surface, as noted above.

On the triplet surface, ^{3}TS1 is much higher in energy than its singlet analog, ^{1}TS1. Because Au^+ ($^3D,6s^15d^9$) has no empty valence orbitals, the simple donor-acceptor process is restricted, leading to the high barrier for ^{3}TS1. The energies of ^{1}TS2 and ^{3}TS2 are quite high because the nearly full occupation of gold does not allow formation of the several covalent bonds needed to stabilize this transition state. The distinction between ^{3}TS2 and ^{1}TS2 is small because these species can be thought of as having a covalent single Au–C and Au–H bonds, which leaves an unpaired electron on C and on the other H. Because the H is not covalently bound to the Au center, the energetic distinction between whether this electron is singlet or triplet coupled to the electron on C is small.

VII. CONCLUSIONS

Ground state Au^+ ions are found to be reactive with methane in endothermic processes. At low energies, dehydrogenation is the only process observed. At high energies, the dominant process is formation of $AuH^+ + CH_3$. This channel is favored over the nearly isoenergetic $AuCH_3^+ + H$ channel because of angular momentum constraints. Excited triplet state Au^+ ions exhibit the same reactions as ground state ions, but with lowered reactivity and different branching ratios.

Analyses of the kinetic energy dependences of the reaction cross sections provide the BDEs of Au^+-CH_3 and Au^+-CH_2. These experimental bond energies are stronger than the corresponding ones of the first-row and second-row transition metals, which is attributed to the effective *sd* hybridization, a consequence of relativistic effects. Our experimental BDEs are found to be in good agreement with B3LYP/HW+ calculations performed here. Literature experimental values for the bond energies to gold ions are substantially refined (Table II).

Calculations are also used to provide a detailed potential energy surface for the $AuCH_4^+$ system. This potential energy surface shows that the reaction of Au^+ ($^1S_0$) with methane proceeds from $Au^+(CH_4)$ adduct (^1A) to form $AuCH_2^+(^1A_1) + H_2$ directly without any transition state involved. AuH^+ and $AuCH_3^+$ can be formed either from $Au^+(CH_4)$ adduct (^1A) or via the oxidative addition of one C–H bond to yield a hydrido-methyl gold intermediate, $H-Au^+-CH_3$ ($^1A'$), and then by simple bond cleavages from this intermediate. This unique reaction mechanism among the third-row transition metal systems is the result of the closed shell $5d^{10}$ electron configuration of Au^+ ($^1S_0$). The potential energy surfaces also show that reaction of Au^+ (^3D) does not couple to the ground state singlet surface and that the dehydrogenation occurs over a barrier (^{3}TS2), both observations in good agreement with experiment.

ACKNOWLEDGMENT

This work is supported by the National Science Foundation, Grant No. CHE-0451477. This paper is in honor of Yuan T. Lee's 70th birthday and in celebration of his many contributions to chemical physics.

[1] M. Haruta, N. Yamada, T. Kobayashi, and S. Iijima, J. Catal. **115**, 301 (1989).
[2] M. S. Chen and D. W. Goodman, Science **306**, 252 (2004).
[3] A. K. Chowdhury and C. L. Wilkins, J. Am. Chem. Soc. **109**, 5336 (1987).
[4] K. K. Irikura and J. L. Beauchamp, J. Am. Chem. Soc. **113**, 2769 (1991).
[5] K. K. Irikura and J. L. Beauchamp, J. Phys. Chem. **95**, 8344 (1991).
[6] P. Mourgues, A. Ferhati, T. B. McMahon, and G. Ohanessian, Organometallics **16**, 210 (1997).
[7] A. Ferhati, T. B. McMahon, and G. Ohanessian, Bull. Soc. Chim. Fr. **130**, 3 (1993).
[8] A. Ferhati, T. B. McMahon, and G. Ohanessian, J. Am. Chem. Soc. **118**, 5997 (1996).
[9] S. W. Buckner, T. J. MacMahon, G. D. Byrd, and B. S. Freiser, Inorg. Chem. **28**, 3511 (1989).
[10] Y. A. Ranasinghe, T. J. MacMahon, and B. S. Freiser, J. Phys. Chem. **95**, 7721 (1991).
[11] W. D. Jones, Acc. Chem. Res. **36**, 140 (2003).
[12] G. Ohanessian, M. J. Brusich, and W. A. Goddard III, J. Am. Chem. Soc. **112**, 7179 (1990).
[13] P. B. Armentrout, S. Shin, and R. J. Liyanage, J. Phys. Chem. A **110**, 1242 (2006).
[14] L. G. Parke, C. S. Hinton, and P. B. Armentrout, Int. J. Mass. Spectrom. **254**, 168 (2006).
[15] M. M. Armentrout, F.-X. Li, and P. B. Armentrout, J. Phys. Chem. A **108**, 9660 (2004).
[16] F.-X. Li, X.-G. Zhang, and P. B. Armentrout, Int. J. Mass. Spectrom. (to be published).
[17] X.-G. Zhang, R. Liyanage, and P. B. Armentrout, J. Am. Chem. Soc. **123**, 5563 (2001).
[18] J. Allison, Inorg. Chem. **34**, 627 (1986); R. R. Squires, Chem. Rev. (Washington, D.C.) **87**, 623 (1987); *Gas-Phase Inorganic Chemistry*, edited by D. H. Russell (Plenum, New York, 1989); K. Eller and H. Schwarz, Chem. Rev. (Washington, D.C.) **91**, 1121 (1991).
[19] For reviews, see P. B. Armentrout and B. L. Kickel, in *Organometallic Ion Chemistry*, edited by B. S. Freiser (Kluwer, Dordrecht, 1996), p. 1; P. B. Armentrout, in *Organometallic Bonding and Reactivity*, Topics in Organometallic Chemistry Vol. 4-I, edited by J. M. Brown and P. Hofmann (Springer-Verlag, Berlin, 1999), p. 1.
[20] R. H. Crabtree, *The Organometallic Chemistry of the Transition Metals*, 2nd ed. (Wiley, New York, 1994).
[21] G. A. Somorjai, *Introduction to Surface Chemistry and Catalysis* (Wiley, New York, 1994).
[22] L. S. Sunderlin and P. B. Armentrout, J. Am. Chem. Soc. **111**, 3845 (1989).
[23] K. K. Irikura and W. A. Goddard III, J. Am. Chem. Soc. **116**, 8733 (1994).
[24] R. Wesendrup, D. Schröder, and H. Schwarz, Angew. Chem., Int. Ed. Engl. **33**, 1174 (1994).
[25] C. Heinemann, R. Wesendrup, and H. Schwarz, Chem. Phys. Lett. **239**, 75 (1995).
[26] M. Pavlov, M. R. A. Blomberg, P. E. M. Siegbahn, R. Wesendrup, C. Heinemann, and H. Schwarz, J. Phys. Chem. A **101**, 1567 (1997).
[27] U. Achatz, M. Beyer, S. Joos, B. S. Fox, G. Niedner-Schatteburg, and V. E. Bondybey, J. Phys. Chem. A **103**, 8200 (1999).
[28] U. Achatz, C. Beyer, S. Joos, B. S. Fox, M. K. Berg, G. Niedner-Schatteburg, and V. E. Bondybey, Chem. Phys. Lett. **320**, 53 (2000).
[29] F. Aguirre, J. Husband, C. J. Thompson, and R. B. Metz, Chem. Phys. Lett. **318**, 466 (2000).
[30] C. Heinemann, W. Koch, and H. Schwarz, Chem. Phys. Lett. **245**, 509 (1995).

[31] C. Heinemann, R. H. Hertwig, R. Wesendrup, W. Koch, and H. Schwarz, J. Am. Chem. Soc. **117**, 495 (1995).
[32] M. C. Holthausen, C. Heinemann, H. H. Cornehl, W. Koch, and H. Schwarz, J. Chem. Phys. **102**, 4931 (1995).
[33] C. Heinemann, H. Schwarz, W. Koch, and K. G. Dyall, J. Chem. Phys. **104**, 4642 (1996).
[34] D. G. Musaev and K. Morokuma, Isr. J. Chem. **33**, 307 (1993).
[35] J. K. Perry, G. Ohanessian, and W. A. Goddard III, Organometallics **13**, 1870 (1994).
[36] Y. Ishikawa, G. L. Malli, and N. C. Pyper, Chem. Phys. Lett. **194**, 481 (1992).
[37] J. Hrušák, S. Afr. J. Chem. **50**, 93 (1997).
[38] S. K. Loh, D. A. Hales, L. Lian, and P. B. Armentrout, J. Chem. Phys. **90**, 5466 (1989).
[39] R. H. Schultz and P. B. Armentrout, Int. J. Mass Spectrom. Ion Process. **107**, 29 (1991).
[40] E. Teloy and D. Gerlich, Chem. Phys. **4**, 417 (1974).
[41] D. Gerlich, Adv. Chem. Phys. **82**, 1 (1992).
[42] K. M. Ervin and P. B. Armentrout, J. Chem. Phys. **83**, 166 (1985).
[43] P. J. Chantry, J. Chem. Phys. **55**, 2746 (1971).
[44] F.-X. Li, K. Gorham, and P. B. Armentrout (unpublished).
[45] W. J. Chesnavich and M. T. Bowers, J. Phys. Chem. **83**, 900 (1979).
[46] N. Aristov and P. B. Armentrout, J. Am. Chem. Soc. **108**, 1806 (1986).
[47] P. B. Armentrout, in *Advances in Gas-Phase Ion Chemistry*, edited by N. G. Adams and L. M. Babcock (JAI, Greenwich, 1992), p. 83.
[48] T. Shimanouchi, *Tables of Molecular Vibrational Frequencies*, Natl. Bur. Stand. (U.S.) Circ. No. NSRDS-NBS39 (U.S. GPO, Washington, D.C., 1972), Vol. I, p. 1.
[49] A. D. Becke, J. Chem. Phys. **98**, 5648 (1993).
[50] C. Lee, W. Yang, and R. G. Parr, Phys. Rev. B **37**, 785 (1988).
[51] M. J. Frisch, G. W. Trucks, H. B. Schlegel *et al.*, GAUSSIAN 98, Revision A.11, Gaussian, Inc., Pittsburgh, PA, 2001.
[52] M. J. Frisch, G. W. Trucks, H. B. Schlegel *et al.*, GAUSSIAN 03, Revision B.02, Gaussian, Inc., Pittsburgh, PA, 2003.
[53] P. J. Hay and W. R. Wadt, J. Chem. Phys. **82**, 299 (1985).
[54] M. C. Holthausen, M. Mohr, and W. Koch, Chem. Phys. Lett. **240**, 245 (1995).
[55] D. Andrae, U. Haeussermann, M. Dolg, H. Stoll, and H. Preuss, Theor. Chim. Acta **77**, 123 (1990).
[56] C. E. Moore, *Atomic Energy Levels*, Natl. Bur. Stand. (U.S.) Circ. No. NSRDS-NBS35 (U.S. GPO, Washington, D.C., 1971), Vol. III, p. 1.
[57] N. Aristov and P. B. Armentrout, J. Phys. Chem. **91**, 6178 (1987).
[58] L. S. Sunderlin and P. B. Armentrout, J. Phys. Chem. **92**, 1209 (1988).
[59] Y.-M. Chen and P. B. Armentrout, J. Phys. Chem. **99**, 10775 (1995).
[60] G. Gioumousis and D. P. Stevenson, J. Chem. Phys. **29**, 294 (1958).
[61] See EPAPS Document No. E-JCPSA6-125-139637 for four tables of energies and structures. This document can be reached via a direct link in the online article's HTML reference section or via the EPAPS homepage (http://www.aip.org/pubservs/epaps.html).
[62] F.-X. Li, F. Liu, and P. B. Armentrout (unpublished).
[63] M. Barysz and P. Pyykkö, Chem. Phys. Lett. **285**, 398 (1998).
[64] J. L. Elkind and P. B. Armentrout, J. Phys. Chem. **90**, 6576 (1986).
[65] R. Georgiadis, E. R. Fisher, and P. B. Armentrout, J. Am. Chem. Soc. **111**, 4251 (1989).
[66] E. R. Fisher and P. B. Armentrout, J. Phys. Chem. **94**, 1674 (1990).
[67] Y.-M. Chen, J. L. Elkind, and P. B. Armentrout, J. Phys. Chem. **99**, 10438 (1995).
[68] Y.-M. Chen and P. B. Armentrout, J. Phys. Chem. **99**, 11424 (1995).
[69] C. Peng and H. B. Schlegel, Isr. J. Chem. **33**, 449 (1994).
[70] C. Peng, P. Y. Ayala, H. B. Schlegel, and M. J. Frisch, J. Comput. Chem. **17**, 49 (1996).
[71] P. Schwerdtfeger, M. Dolg, W. H. E. Schwarz, G. A. Bowmaker, and P. D. W. Boyd, J. Chem. Phys. **91**, 1762 (1989).
[72] J. Hrušák, R. H. Hertwig, D. Schröder, P. Schwerdtfeger, W. Koch, and H. Schwarz, Organometallics **14**, 1284 (1995).